HAL
open science

Relaxation mechanism in NiFe thin films driven by spin angular momentum absorption throughout the antiferromagnetic phase transition in native surface oxides

L. Frangou, G. Forestier, S. Auffret, S. Gambarelli, V. Baltz

▶ **To cite this version:**

L. Frangou, G. Forestier, S. Auffret, S. Gambarelli, V. Baltz. Relaxation mechanism in NiFe thin films driven by spin angular momentum absorption throughout the antiferromagnetic phase transition in native surface oxides. Physical Review B: Condensed Matter and Materials Physics (1998-2015), 2017, 95, pp.054416. 10.1103/PhysRevB.95.054416 . hal-01568743v2

HAL Id: hal-01568743

https://hal.science/hal-01568743v2

Submitted on 19 May 2019

HAL is a multi-disciplinary open access archive for the deposit and dissemination of scientific research documents, whether they are published or not. The documents may come from teaching and research institutions in France or abroad, or from public or private research centers.

L'archive ouverte pluridisciplinaire **HAL**, est destinée au dépôt et à la diffusion de documents scientifiques de niveau recherche, publiés ou non, émanant des établissements d'enseignement et de recherche français ou étrangers, des laboratoires publics ou privés.

Relaxation mechanism in NiFe thin films driven by spin angular momentum absorption throughout the antiferromagnetic phase transition in native surface oxides

L. Frangou,[1] G. Forestier,[1] S. Auffret,[1] S. Gambarelli,[2] and V. Baltz[1,*]
[1]*SPINTEC, Univ. Grenoble Alpes/CNRS/INAC-CEA, F-38000 Grenoble, France*
[2]*SYMMES, Univ. Grenoble Alpes/INAC-CEA, F-38000 Grenoble, France*
(Received 9 December 2016; revised manuscript received 26 January 2017; published 14 February 2017)

We report an alternative mechanism for the physical origin of the temperature-dependent ferromagnetic relaxation observed in bare permalloy (NiFe) thin films. Through spin-pumping experiments, we demonstrate that the peak in the temperature dependence of NiFe damping can be understood in terms of enhanced absorption of spin angular momentum at the magnetic phase transition in native antiferromagnetic surface-oxidized layers. These results suggest some avenues for the investigation of an incompletely understood phenomenon in physics.

DOI: 10.1103/PhysRevB.95.054416

In physical systems, damping characterizes the losses associated with out-of-equilibrium vibration dynamics [1,2]. In the field of spintronics, which relies on the spin-dependent transport properties of matter [3–5], magnetic damping is one of the key parameters as it regulates oscillations and switches in magnetization direction in any magnetic material [6,7]. Magnetic damping plays this role with all kinds of stimuli, whether the dynamics of magnetization is excited through an electromagnetic wave [8], an electrical current [9], or a spin current [10]. Damping in typical ferromagnetic materials has been thoroughly experimentally characterized through measurements of ferromagnetic resonance spectra and determination of their linewidths [11]. Several mechanisms have been proposed to explain these findings [11]. However, the basic mechanisms behind some magnetic relaxation behavior remain unclear even in common magnetic materials. For example, CoFe alloys were recently theoretically predicted [12] and experimentally demonstrated [13] to display ultralow damping which was previously believed to be unachievable in metallic ferromagnets. In this article, inspired by recent theoretical and experimental findings related to spin pumping [14–19], we chose to investigate bare permalloy (NiFe) in an attempt to determine the incompletely understood origin of their nonmonotonous temperature dependence of ferromagnetic damping [20–25]. More specifically, typical 3*d* transition metals (Co, Ni, Fe) and associated alloys (including NiFe) frequently show a minimum in the temperature dependence of their damping [26,27]. It is now accepted that a conductivitylike term related to intraband scattering dominates local intrinsic damping at low temperatures, whereas a resistivitylike term due to interband scattering takes over at higher temperatures [27]. Sometimes for NiFe, a contrasting pronounced maximum was unexpectedly observed in the temperature-dependent damping [20]. This finding, and the reasons for it, remain controversial and are still being discussed. It has been suggested that the temperature-dependent reorientation of NiFe surface spins from in plane to out of plane could account for the maximum damping observed [22–24]. However, recent evidence indicates that spin reorientation may occur at a much lower temperature than the maximum damping [28]. An alternative mechanism was also proposed involving slow relaxation on paramagnetic impurities present in, or adjacent to, the oscillating ferromagnetic material [20,21,29,30]. In this process, the oscillations in the magnetization of the ferromagnet modulate how the energy splits between impurity levels. Subsequent relaxation of the impurities influences ferromagnetic damping. In fact, if not protected from oxidation due to exposure to air, a few monolayers of the NiFe layer will naturally oxidize to form a passivating oxide layer (NiFeOx). This layer contains a complex mixture of NiO and FeO antiferromagnetic alloys with variable stoichiometry gradients [25]. In this context, the potential influence of relaxation of interface paramagnetic impurities in bilayers where a ferromagnet is exchange biased to an antiferromagnet was considered in several studies [31–34]. However, the results of these studies led to divergent mechanisms being presented to explain the temperature dependence of the relaxation rate for impurities [31–34]. Beyond paramagnetic impurities or exchange-bias interactions, the presence of NiFe antiferromagnetic surface oxides raises the question of how spin angular momentum is absorbed by the antiferromagnetic layer itself [35,36]. In this process, transfer/sink and propagation of spin angular momentum involves magnons from the oscillating ferromagnet feeding into the antiferromagnet, due to magnetic coupling [37,38]. The end result is an overall enhancement of the total damping of the ferromagnet [35,36]. In addition, near the phase transition for the magnetic order of the antiferromagnetic layer, i.e., around its Néel temperature, the magnetic fluctuations were shown to lead to a maximum spin-pumping efficiency [16–18]. The origin of this phenomenon was corroborated by calorimetry [16,39] and neutron diffraction measurements [18].

In this work, we investigated whether enhanced spin angular momentum absorption at the magnetic phase transition of native interface- and surface-oxidized layers could be an alternative mechanism explaining the temperature-dependent ferromagnetic relaxation of bare NiFe. We examined temperature-dependent ferromagnetic relaxation in NiFe thin films, and how it was affected by native oxidation of the NiFe layer and the number of native oxide layers surrounding the NiFe (two, one, or none). Spin-pumping experiments were performed at various temperatures on a first series of samples consisting of Si/SiO_2(500)/NiFe(8) (short name: SiO_2/NiFe), Si/SiO_2(500)/NiFe(8)/Cu(3)/Al(2) (short name: SiO_2/NiFe/Cu/Al), Si/SiO_2(500)/Cu(6)/NiFe(8)

*vincent.baltz@cea.fr

 ©2017 American Physical Society

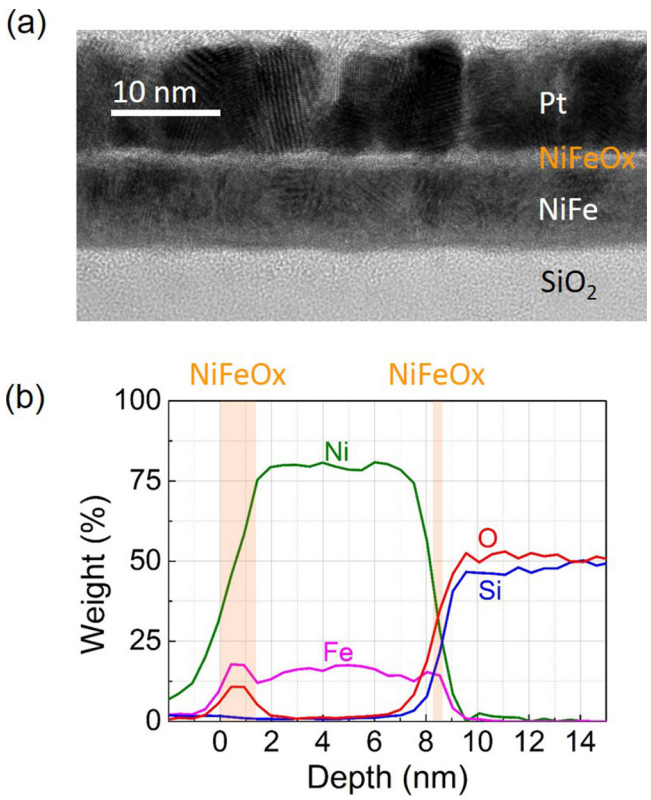

FIG. 1. (a) Transmission electron microscopy image (TEM) and (b) energy-dispersive x-ray spectroscopy (EDX) data for a SiO_2/NiFe sample. Samples were capped with Pt in preparation for the TEM experiment.

(short name: SiO_2/Cu/NiFe), and Si/SiO_2(500)/Cu(6)/NiFe(8)/Cu(3)/Al(2) (short name: SiO_2/Cu/NiFe/Cu/Al) multilayers. All thicknesses are given in nanometers. Stacks were deposited on thermally oxidized silicon substrates [Si/SiO_2(500)] at room temperature by dc-magnetron sputtering. The NiFe layer was deposited from a permalloy target [$Ni_{81}Fe_{19}$ (at.%)]. An Al(2) cap was added, forming a protective passivating AlOx film, to block oxidization by air in some samples. The other samples were exposed to air. Data recorded after a week and after a month overlapped, indicating that oxidation has reached a maximum after a week. Uncapped layers were therefore exposed to air for a minimum of one week before any measurements were performed. Transmission electron microscopy (TEM) analysis [Fig. 1(a)] was used to view oxidation of the NiFe layer in the SiO_2/NiFe stack. After exposure to air, some sample pieces were capped with Pt in preparation for the TEM experiment. This cap protects the sample's surface from damage during the thinning and polishing steps required for TEM. It also enhances the TEM contrast around the sample surface. Results of the TEM investigations indicated a NiFe surface oxide (NiFeOx) produced by NiFe oxidation in air. The thickness of the NiFeOx surface oxide, as determined from the TEM data was approximately 1.6 ± 0.2 nm. The margin of error corresponds to typical errors in thickness measurements performed at various locations in TEM images. The NiFeOx thickness value is in line with data from the literature, where passivating surface oxides were reported to measure nanometers thick [25]. Results from energy-dispersive x-ray spectroscopy (EDX) measurements [Fig. 1(b)] confirm the presence of a surface-oxidized layer and reveal the presence of another native oxidized layer at the interface between the SiO_2 and NiFe layers. This lower oxide layer was not visible in the TEM image due to a lack of contrast with the SiO_2 underlayer. Unlike the top oxide, this bottom oxide is not produced due to oxidation in air. Rather, it forms naturally at the SiO_2/NiFe interface, likely activated by the Ni and Fe atoms when they interact with the SiO_2 surface during sputter deposition. The presence and thickness (around 0.3 ± 0.2 nm) of this bottom oxide layer was determined from the horizontal shift in the oxygen and silicon traces in EDX data [visible in Fig. 1(b)]. Indeed, Fig. 1(b) represents atomic weight as a function of sample depth. Since the O signal rises before the Si signal, some oxygen atoms must have mixed with the NiFe layer. The shift between the Si and O traces along the sample depth corresponds to the thickness of this bottom NiFeOx layer. The margin of error corresponds to typical errors reported for EDX data due to measurements performed at different locations in the film. From the EDX data, we also calculated that in the SiO_2/NiFe sample, the Ni and Fe atoms extend over a total thickness of around 8.1 ± 0.2 nm. Complementary EDX measurements performed on a SiO_2/NiFe/Cu/Al sample, where the NiFe layer was not air oxidized, indicated that the Ni and Fe atoms also extend over a total thickness of around 8 ± 0.3 nm. This observation suggests negligible expansion of the lattice parameter for the oxide layer in SiO_2/NiFe samples. The margins of error reported here give an estimate of the typical error level between nominal and actual thickness. To sum up, from the TEM and EDX experiments we can conclude that the initial SiO_2/NiFe, SiO_2/NiFe/Cu/Al, SiO_2/Cu/NiFe, and SiO_2/Cu/NiFe/Cu/Al multilayers are in fact the following stacks SiO_2/ NiFeOx(0.3)/NiFe/NiFeOx (1.6), SiO_2/NiFeOx(0.3)/NiFe/Cu/AlOx, SiO_2/Cu/NiFe/NiFeOx(1.6), and SiO_2/Cu/NiFe/Cu/AlOx, respectively.

We next investigated the magnetic nature of the surface-oxidized layers by measuring hysteresis loops at various temperatures using a magnetometer [Fig. 2(a)]. These results show a loop shift (H_E) along the axis of the magnetic field, demonstrating magnetic exchange-bias interactions [40,41] between the NiFe ferromagnetic layer and the NiFeOx surface-oxidized layer. These data confirmed the antiferromagnetic nature of the top surface-oxidized layer. The data presented in Fig. 2(b) further indicated that H_E decreases as the temperature rises. The ferromagnetic/antiferromagnetic blocking temperature (T_B) can be extracted from H_E vs T by determining the temperature at which H_E vanishes [40,41]. T_B is expected to be much smaller than the critical temperature (T_{crit}) for the antiferromagnetic-to-paramagnetic transition [40,41], and for exchange-bias interactions with the top NiFeOx(1.6) layer, it was found to be about 15 K (see data for the SiO_2/Cu/NiFe and SiO_2/NiFe samples). This relationship can be explained as T_B is linked to the interfacial exchange interactions between the ferromagnet and the antiferromagnet, whereas T_{crit} relates to the exchange stiffness between all antiferromagnetic moments. For exchange-bias interactions with the lower NiFeOx(0.3) layer (see data for the SiO_2/NiFe/Cu sample), T_B was determined to be sub-K. Its value could not be measured based on the data shown in Fig. 2(b) due to the fact that

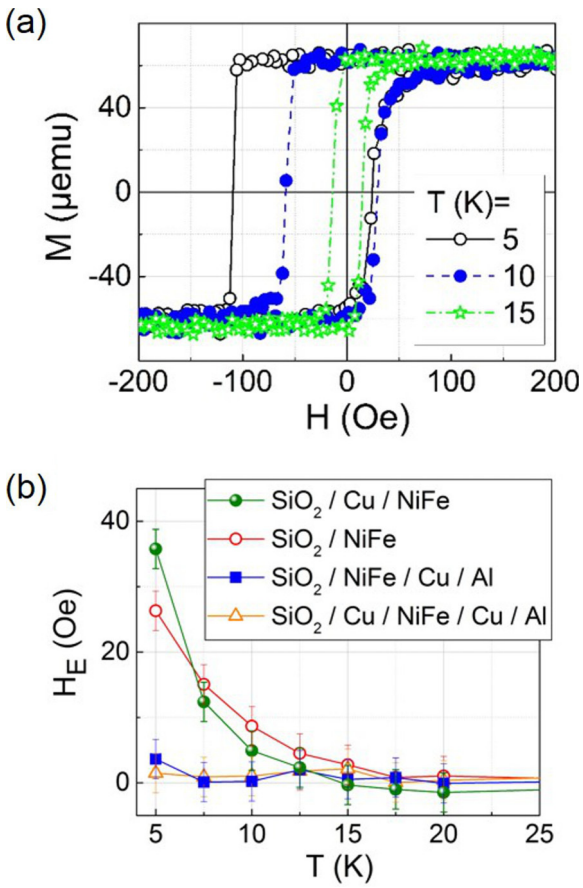

FIG. 2. (a) Representative magnetization (M) vs field (H) hysteresis loops at different temperatures for a SiO_2/Cu/NiFe sample. (b) Temperature (T) dependence of the hysteresis loop shift (H_E).

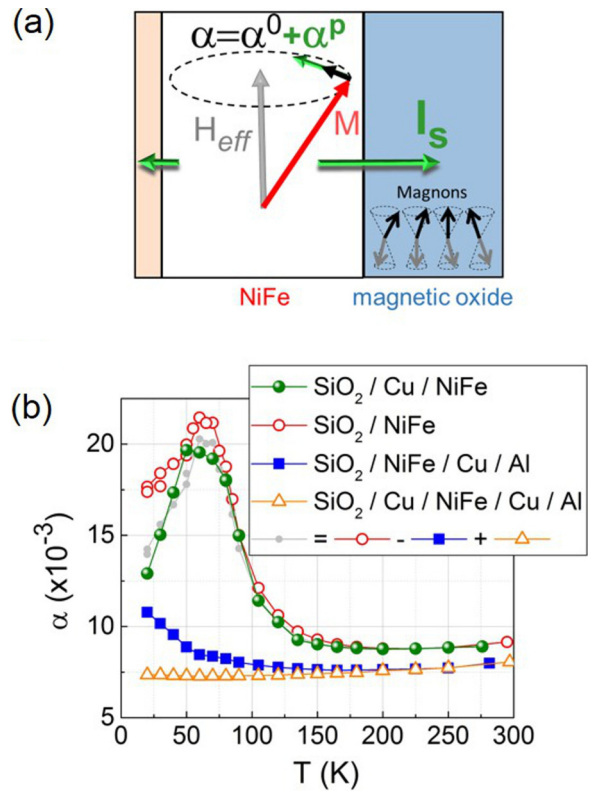

FIG. 3. (a) Diagrammatic representation of the spin-pumping experiment. (b) Temperature (T) dependence of the NiFe layer Gilbert damping (α). The NiFe layer is surrounded by two, one, or no native oxide layers. When the NiFe is deposited directly on SiO_2 a 0.3-nm-thick NiFeOx naturally forms at the SiO_2/NiFe interface, activated by the Ni and Fe atoms when interacting with the SiO_2 surface during sputter deposition. When the NiFe layer is left uncapped it naturally undergoes oxidation due to contact with air, resulting in a 1.6-nm-thick NiFeOx surface layer.

the lower NiFeOx(0.3) oxide layer is very thin and displays a reduced T_{crit}. Note that for the ultrathin NiFeOx(0.3) layer, T_{crit} probably describes a frozen-to-liquid spin transition. Results confirming the reduced value of T_{crit} will be discussed below.

Spin-pumping experiments [Fig. 3(a)] and related series of ferromagnetic resonance spectra were recorded for temperatures (T) ranging between 20 and 300 K, using a continuous-wave electron paramagnetic resonance spectrometer operating at 9.6 GHz fitted with a cavity. For each temperature the Gilbert damping (α) was determined by fitting the NiFe resonance spectrum to a Lorenzian. The value of α was extracted from $\alpha(T) = [\Delta H_{pp}(T) - \Delta H_0(300\,\mathrm{K})]\sqrt{3}|\gamma|/(2\omega)$, where ΔH_{pp} is the peak-to-peak linewidth for the spectrum, γ is the gyromagnetic ratio, and ω is the angular frequency [42]. ΔH_0 relates to spatial variations in the magnetic properties. This parameter was determined from standard ΔH_{pp} vs $\omega/2\pi$ plots using a separate, broadband coplanar waveguide operating at room temperature for frequencies ranging between 2 and 24 GHz [42]. For bare NiFe films similar to those described above, ΔH_0 was previously found to be a temperature-invariant parameter [43]. Figure 3(b) shows α plotted against temperature. The pronounced maximum at $T = 70$ K corresponds to the top NiFeOx(1.6) layer resulting from natural oxidation in air (see data for the SiO_2/NiFe and SiO_2/Cu/NiFe samples). The amplitude of this maximum was threefold the amplitude measured at 300 K. A less pronounced contribution is visible at lower temperatures in samples containing the bottom NiFeOx(0.3) layer, where the NiFe become naturally oxidized due to contact with the SiO_2 layer (see data for the SiO_2/NiFe/Cu/Al sample). When the NiFe layer was isolated from oxygen atoms on both sides (in the SiO_2/Cu/NiFe/Cu/Al sample) no such maxima were observed.

Since the oxidized layers are magnetic, the NiFe damping is the sum of local intrinsic damping (α^0) that can be described by intraband and interband scattering [27] and additional nonlocal damping ($\alpha^{p,i}$) associated with the surface/interface NiFeOx oxide(s) acting as a spin absorber for angular momentum. The temperature dependence of α can thus be expressed as $\alpha(T) = \alpha^0(T) + \sum_i \alpha^{p,i}(T)$ [14,35,36], where i accounts for the uppermost and/or lowermost NiFeOx spin absorber. Data obtained with the SiO_2/Cu/NiFe/Cu/Al sample (no spin absorber) give the temperature dependence of the local intrinsic NiFe Gilbert damping [$\alpha_{SiO_2/Cu/NiFe/Cu/Al}(T) = \alpha^0(T)$] with a detectable conductivitylike to resistivitylike progression [26,27]. From Fig. 3(b), we can thus conclude that the temperature dependence of α^0 can be neglected, but that $\alpha^{p,i}$ is highly temperature dependent. The nonlocal damping is related to the spin mixing conductance across the NiFe/NiFeOx(1.6) and/or NiFeOx(0.3)/NiFe interfaces

(g_s^i) as presented in [14] by $\alpha^{p,i}(T) = \frac{1}{S_0 N_{\rm SI}} g_s^i(T)$, where S_0 is the norm of the spin operator, and $N_{\rm SI}$ is the number of lattice sites in the NiFe spin injector (SI). The spin mixing conductance across the interface is linked to the magnetic susceptibility of the spin absorber [14] via $g_s^i(T) = \frac{2J_{sd}^2 S_0^2 N_{\rm int}}{\hbar^2 N_{\rm SA}^i} \sum_k \frac{1}{\Omega_{rf}} {\rm Im}\chi_k^{R,i}(\Omega_{rf},T)$, where $N_{\rm int}$ is the number of spins localized at the interface, $N_{\rm SA}^i$ is the number of lattice sites in the spin absorber (SA) i, J_{sd} is the s-d exchange interaction at the SI/SA interface, k is the wave vector, and Ω_{rf} is the angular frequency of NiFe at resonance. The temperature-dependent dynamic spin susceptibility of the spin absorber can be represented by $\chi_k^{R,i}(\Omega_{rf},T)$. As a result, the nonlocal damping is given by $\alpha^{p,i}(T) = \frac{2J_{sd}^2 S_0 N_{\rm int}}{\hbar^2 N_{\rm SA}^i N_{\rm SI}} \sum_k \frac{1}{\Omega_{rf}} {\rm Im}\chi_k^{R,i}(\Omega_{rf},T)$. The spin susceptibility of antiferromagnetic materials is known to display a maximum around the critical temperature for the magnetic phase transition due to magnetic fluctuations. This transition results in enhanced spin mixing conductance across the interface (g_s^i). In other words, magnetic fluctuations in the spin absorber open more conduction channels across the interface, which translates into enhanced spin angular momentum absorption ($\alpha^{\rm p,i}$) and therefore into maximal NiFe total damping (α), as observed in Fig. 3(b). From data for SiO_2/Cu/NiFe, where $\alpha_{\rm SiO_2/Cu/NiFe}(T) = \alpha^0(T) + \alpha^{p,\rm NiFeOx(1.6)}(T)$, we deduced the Néel temperature for the magnetic phase transition of the top 1.6-nm-thick NiFeOx oxide, at approximately 70 K. From the SiO_2/NiFe/Cu/Al in Fig. 3(b), where $\alpha_{\rm SiO_2/NiFe/Cu/Al}(T) = \alpha^0(T) + \alpha^{p,\rm NiFeOx(0.3)}(T)$, we concluded that the critical temperature for the phase transition of the lowermost 0.3-nm-thick NiFeOx oxide, which formed naturally at the interface between the NiFe and SiO_2 layers, is less than 20 K. We infer that this temperature is actually well below 20 K, and probably sub-K since the amplitude of the damping peak for the 0.3-nm-thick NiFeOx oxide is expected to be fivefold (1.6/0.3) that of the 1.6-nm-thick oxide. This difference can be explained by the fact that $\alpha^{\rm p}$ is inversely proportional to the number of lattice sites in the spin absorber ($N_{\rm SA}$). Finally, data for the SiO_2/NiFe sample relate to $\alpha_{\rm SiO_2/NiFe}(T) = \alpha^0(T) + \alpha^{p,\rm NiFeOx(0.3)}(T) + \alpha^{p,\rm NiFeOx(1.6)}(T)$. From the four relations above between $\alpha_{\rm SiO_2/NiFe}$, $\alpha_{\rm SiO_2/NiFe/Cu/Al}$, $\alpha_{\rm SiO_2/Cu/NiFe/Cu/Al}$, and $\alpha_{\rm SiO_2/Cu/NiFe}$; and α^0, $\alpha^{p,\rm NiFeOx(0.3)}$, and $\alpha^{p,\rm NiFeOx(1.6)}$ our experimental data should confirm the following equation: $\alpha_{\rm SiO_2/NiFe} - \alpha_{\rm SiO_2/NiFe/Cu/Al} + \alpha_{\rm SiO_2/Cu/NiFe/Cu/Al} = \alpha_{\rm SiO_2/Cu/NiFe}$. The data shown in Fig. 3(b) clearly confirm the equation, where the small gray filled circles ($\alpha_{\rm SiO_2/NiFe} - \alpha_{\rm SiO_2/NiFe/Cu/Al} + \alpha_{\rm SiO_2/Cu/NiFe/Cu/Al}$) satisfactorily overlap the green circles ($\alpha_{\rm SiO_2/Cu/NiFe}$). This verification further supports absorption of spin angular momentum at the magnetic phase transition of the native surface-oxidized layers as an alternative mechanism explaining the temperature-dependent ferromagnetic relaxation of bare NiFe, while also indicating satisfactory reproducibility of data and native oxidation from sample to sample.

We note here that it is essential that transfer and propagation of spin angular momentum directly involves magnonic transport. In other words, the NiFeOx must be fed by spin waves through direct magnetic coupling with NiFe. The difference in spin-pumping efficiency by a

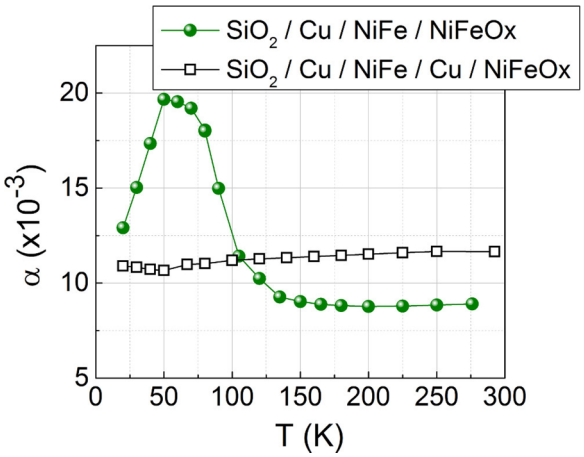

FIG. 4. Temperature (T) dependence of damping (α) of a NiFe ferromagnet directly coupled to a 1.6-nm-thick antiferromagnetic NiFeOx or separated by a 3-nm-thick Cu layer. In the SiO_2/Cu/NiFe/NiFeOx sample, NiFeOx results from the native oxidation of NiFe(8 nm), creating a passivating 1.6-nm-thick layer. In the SiO_2/Cu/NiFe/Cu/NiFeOx sample, NiFeOx results from complete native oxidation of a NiFe(1.6 nm) layer.

~1.6-nm-thick antiferromagnetic NiFeOx directly coupled to NiFe, or separated from the ferromagnetic NiFe layer by a 3-nm-thick Cu layer is shown in Fig. 4. The enhanced damping at 70 K due to the magnetic phase transition of the NiFeOx is clearly observed in the case of direct magnonic transport but is suppressed when the Cu breaks the direct magnetic interaction between NiFe and NiFeOx. In the latter case, spin transport is mediated by a purely electronic transport regime through Cu. As the spin diffusion length for Cu is much longer than 3 nm, spin propagation will not be altered by passing through this layer. However, from the data shown in Fig. 4 virtually no spin angular momentum is transmitted to the NiFeOx. The presence of intermediate copper oxide at the Cu/NiFeOx interface cannot be excluded and may also account for the overall increase of α.

We further investigated how $T_{\rm crit}$ is influenced by the thickness of the native oxide. Spin-pumping experiments were performed at various temperatures on a second series of samples, where NiFe ($t_{\rm NiFe}$) layers were grown on Si/SiO_2, naturally oxidized by air for a week before adding another NiFe(8) layer, which was left uncapped. $t_{\rm NiFe}$ is the thicknesses of the bottom NiFe layer (0.5, 1, or 1.5 nm). Based on the results presented above, the lowermost NiFe layer is expected to be fully oxidized in air. The samples therefore consisted of a Si/SiO_2/NiFeOx($t_{\rm NiFeOx}$)/NiFe/NiFeOx(1.6) with nominal $t_{\rm NiFeOx} = 0.5, 1$, or 1.5 nm. The NiFe layer is therefore influenced by two spin angular momentum absorbers, and its damping will correspond to the sum of local intrinsic damping, nonlocal extrinsic damping due to spin absorption by the lower NiFeOx($t_{\rm NiFeOx}$), and nonlocal extrinsic damping due to spin absorption by the upper NiFeOx(1.6) layer: $\alpha(T) = \alpha^0(T) + \alpha^{p,\rm NiFeOx(t_{NiFeOx})}(T) + \alpha^{p,\rm NiFeOx(1.6)}(T)$. Due to fluctuations of the antiferromagnetic order, $\alpha^{p,\rm NiFeOx(t_{NiFeOx})}(T)$ and $\alpha^{p,\rm NiFeOx(1.6)}(T)$ are expected to show a maximum at the magnetic phase transition for the NiFeOx($t_{\rm NiFeOx}$) and NiFeOx(1.6) layer, respectively. Figure 5(a) shows α plotted

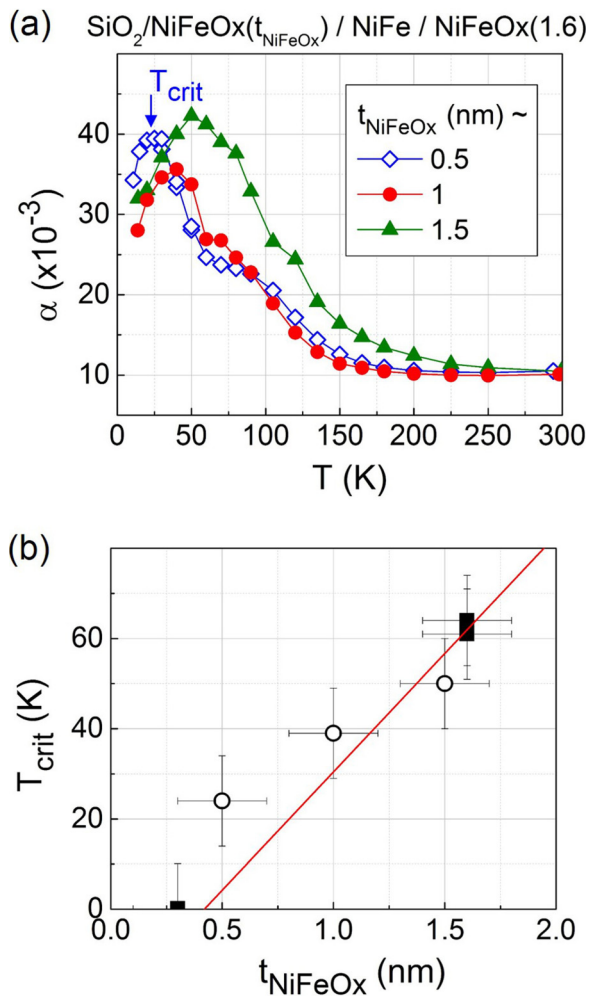

FIG. 5. (a) Temperature (T) dependence of the Gilbert damping (α) of the NiFe layer on temperature (T) in SiO_2/NiFeOx(t_{NiFeOx})/NiFe/NiFeOx(1.6) (nm) multilayers. (b) Thickness dependence of the critical temperature (T_{crit}) for the magnetic phase transition of the oxidized NiFe layer. Open circles represent data deduced from (a). Full squares represent data deduced from Fig. 3(b). Line fitting was based on the equation presented by Zhang *et al.* [44] in the thin-layer regime for a $(NiO)_{81}(FeO)_{19}$ alloy.

against temperature for these multilayers. The data indicate two contributions to α for samples containing the 0.5- and 1-nm-thick lowermost NiFeOx layers. In line with the results presented above, the contribution (shoulder) at around 70 K corresponds to the magnetic phase transition of the uppermost NiFeOx(1.6) layer. The expected maximum in damping actually overlaps with the tail of the peak that can be observed at lower temperatures (at around 25 and 40 K for $t_{NiFeOx} = 0.5$ and 1 nm, respectively). The peak at the lower temperature corresponds to the magnetic phase transition of the lowermost NiFeOx(0.5 or 1) layer. From Fig. 5(a), we observe that the contribution of the phase transition of the lower layer shifts towards higher temperatures as its thickness increases. With the SiO_2/NiFeOx(1.5)/NiFe/NiFeOx(1.6) sample, the NiFe is sandwiched between two similar NiFeOx layers. The top and bottom NiFeOx layers in the Si/SiO_2/NiFeOx(1.5)/NiFe/NiFeOx(1.6) sample therefore absorb similar amounts of spin current on both sides [$\alpha^{p,\mathrm{NiFeOx(1.5)}}(T) \sim \alpha^{p,\mathrm{NiFeOx(1.6)}}(T)$] and share a similar T_{crit}, around 70 K, as previously deduced for the NiFeOx(1.6) layer [Fig. 3(b)]. As a result, the peaks corresponding to the magnetic phase transitions for the top NiFeOx(1.5) and bottom NiFeOx(1.6) layers overlapped. The peak's amplitude for the Si/SiO_2/NiFeOx(1.5)/NiFe/NiFeOx(1.6) sample with two similar spin absorbers [Fig. 5(a)] was effectively close to twice the amplitude of the peak for the SiO_2/Cu/NiFe/NiFeOx(1.6) sample [nominal SiO_2/Cu/NiFe in Fig. 3(b)]. Satisfactory reproducibility of data and native oxidation can also be concluded from these data. Figure 5(b) illustrates how the critical temperature for the NiFeOx layer, regardless of its actual nature, is directly proportional to its thickness. This linear relationship is in line with theories on finite size scaling of magnetic phase transitions [44,45] whereby $T_{crit}(t_{NiFeOx}) = T_N(\mathrm{bulk})(t_{NiFeOx}\text{-}d)/(2n_0)$, with T_N(bulk) as the bulk Néel temperature of the NiFeOx layer, t_{NiFeOx} as its thickness, d as its lattice parameter, and n_0 as its phenomenological interspin correlation length. This corroboration of theory supports the fact that what we actually measured is the result of a magnetic phase transition of the NiFeOx layer, which was formed by natural oxidation of NiFe. Unfortunately, our data cannot be readily fitted to the model because the actual nature of the NiFeOx layer is complex, as it is composed of a mixture of different phases including NiO and FeO alloys, and variations in thickness due to the oxidation rate [25], nor can cluster formations be excluded. The red line in Fig. 4(b) represents a fit for the $Ni_{81}Fe_{19}Ox$ layer determined by considering it as a $(NiO)_{81}(FeO)_{19}$ alloy (approximately proportional to the initial Ni-to-Fe atomic ratio). We used $T_N(\mathrm{bulk}) = 0.81T_{N,NiO}(\mathrm{bulk}) + 0.19T_{N,FeO}(\mathrm{bulk})$ for fitting, with $T_{N,NiO}(\mathrm{bulk}) = 520$ K, $T_{N,FeO}(\mathrm{bulk}) = 200$ K [40], $d = 0.81d_{NiO} + 0.19d_{FeO}$, $d_{NiO} = 0.417$ nm, and d_{FeO}=0.433 nm. This fit is shown to give the reader an idea of what such a simple and straightforward assumption would give. The fit agreed with our data to a satisfactory extent, and returned $n_0 = 4.4$ nm (approximately ten monolayers), which is typical for ordered magnetic films [25].

In conclusion, the main contribution of this paper is the experimental evidence it presents supporting an alternative mechanism explaining the incompletely understood physical origin of the temperature-dependent ferromagnetic relaxation of bare permalloy. Our results demonstrated that the peak in temperature dependence of permalloy damping can be understood in terms of enhanced absorption of spin angular momentum at the antiferromagnetic-to-paramagnetic phase transition of its naturally oxidized surface layers. These findings open perspectives for further investigations, since a multitude of magnetic materials naturally form antiferromagnetic spin absorbers upon oxidation in air or when alloys form with elements contained in neighboring layers.

We acknowledge financial support from the French National Agency for Research (ANR JCJC ASTRONICS, Grant No. ANR-15-CE24-0015-01). We also thank M. Gallagher-Gambarelli for critical reading of the manuscript.

[1] L. Landau and E. Lifshitz, Phys. Z. Sowjetunion **8**, 101 (1935).
[2] T. L. Gilbert, IEEE Trans. Magn. **40**, 3443 (2004).
[3] I. Žutić, J. Fabian, and S. Das Sarma, Rev. Mod. Phys. **76**, 323 (2004).
[4] T. Jungwirth, X. Marti, P. Wadley, and J. Wunderlich, Nat. Nanotechnol. **11**, 231 (2016).
[5] V. Baltz, A. Manchon, M. Tsoi, T. Moriyama, T. Ono, and Y. Tserkovnyak, arXiv:1606.04284.
[6] M. Farle, Rep. Prog. Phys. **61**, 755 (1999).
[7] H. V. Gomonay and V. M. Loktev, Low Temp. Phys. **40**, 22 (2014).
[8] A. Kirilyuk, A. V. Kimel, and T. Rasing, Rev. Mod. Phys. **82**, 2731 (2010).
[9] D. C. Ralph and M. D. Stiles, J. Magn. Magn. Mater. **320**, 1190 (2008).
[10] *Spin Current*, edited by S. Maekawa, S. O. Valenzuela, E. Saitoh, and T. Kimura, Series on Semiconductor Science and Technology (Oxford University Press, Oxford, 2012).
[11] B. Heinrich, *Ultrathin Magnetic Structures III* (Springer, New York, 2005).
[12] S. Mankovsky, D. Ködderitzsch, G. Woltersdorf, and H. Ebert, Phys. Rev. B **87**, 014430 (2013).
[13] M. A. W. Schoen, D. Thonig, M. L. Schneider, T. J. Silva, H. T. Nembach, O. Eriksson, O. Karis, and J. M. Shaw, Nat. Phys. **12**, 839 (2016).
[14] Y. Ohnuma, H. Adachi, E. Saitoh, and S. Maekawa, Phys. Rev. B **89**, 174417 (2014).
[15] R. Khymyn, I. Lisenkov, V. S. Tiberkevich, A. N. Slavin, and B. A. Ivanov, Phys. Rev. B **93**, 224421 (2016).
[16] L. Frangou, S. Oyarzun, S. Auffret, L. Vila, S. Gambarelli, and V. Baltz, Phys. Rev. Lett. **116**, 077203 (2016).
[17] W. Lin, K. Chen, S. Zhang, and C. L. Chien, Phys. Rev. Lett. **116**, 186601 (2016).
[18] Z. Qiu, J. Li, D. Hou, E. Arenholz, A. T. N'Diaye, A. Tan, K.-I. Uchida, K. Sato, Y. Tserkovnyak, Z. Q. Qiu, and E. Saitoh, Nat. Commun. **7**, 12670 (2016).
[19] S. M. Rezende, R. L. Rodríguez-Suárez, and A. Azevedo, Phys. Rev. B **93**, 054412 (2016).
[20] C. E. Patton and C. H. Wilts, J. Appl. Phys. **38**, 3537 (1967).
[21] V. L. Safonov and H. N. Bertram, J. Appl. Phys. **94**, 529 (2003).
[22] M. Dıáz De Sihues, P. J. Silva, and J. R. Fermin, Phys. B **354**, 361 (2004).
[23] J. F. Sierra, V. V. Pryadun, F. G. Aliev, S. E. Russek, M. García-Hernández, E. Snoeck, and V. V. Metlushko, Appl. Phys. Lett. **93**, 172510 (2008).
[24] J. F. Sierra, V. V. Pryadun, S. E. Russek, M. García-Hernández, F. Mompean, R. Rozada, O. Chubykalo-Fesenko, E. Snoeck, G. X. Miao, J. S. Moodera, and F. G. Aliev, J. Nanosci. Nanotechnol. **11**, 7653 (2011).
[25] R. A. Pollak and C. H. Bajorek, J. Appl. Phys. **46**, 1382 (1975).
[26] S. M. Bhagat and P. Lubitz, Phys. Rev. B **10**, 179 (1974).
[27] K. Gilmore, Y. U. Idzerda, and M. D. Stiles, Phys. Rev. Lett. **99**, 027204 (2007).
[28] Y. Zhao, Q. Song, S.-H. Yang, T. Su, W. Yuan, S. S. P. Parkin, J. Shi, and W. Han, Sci. Rep. **6**, 22890 (2016).
[29] V. L. Safonov and H. N. Bertram, Phys. Rev. B **61**, R14893(R) (2000).
[30] A. M. Clogston, Bell Syst. Tech. J. **34**, 739 (1955).
[31] P. Lubitz, J. J. Krebs, M. M. Miller, and S. Cheng, J. Appl. Phys. **83**, 6819 (1998).
[32] P. Lubitz, M. Rubinstein, J. J. Krebs, and S. F. Cheng, J. Appl. Phys. **89**, 6901 (2001).
[33] R. D. McMichael, C. G. Lee, M. D. Stiles, F. G. Serpa, P. J. Chen, and W. F. Egelhoff, J. Appl. Phys. **87**, 6406 (2000).
[34] J. Dubowik, F. Stobiecki, I. Gościańska, Y. P. Lee, A. Paetzold, and K. Röll, Eur. Phys. J. B **45**, 283 (2005).
[35] Y. Tserkovnyak, A. Brataas, and G. E. W. Bauer, Phys. Rev. Lett. **88**, 117601 (2002).
[36] Y. Tserkovnyak, A. Brataas, G. E. W. Bauer, and B. I. Halperin, Rev. Mod. Phys. **77**, 1375 (2005).
[37] C. Hahn, G. De Loubens, V. V. Naletov, J. Ben Youssef, O. Klein, and M. Viret, Europhys. Lett. **108**, 57005 (2014).
[38] H. Wang, C. Du, P. C. Hammel, and F. Yang, Phys. Rev. Lett. **113**, 097202 (2014).
[39] D. Petti, E. Albisetti, H. Reichlová, J. Gazquez, M. Varela, M. Molina-Ruiz, A. F. Lopeandía, K. Olejník, V. Novák, I. Fina, B. Dkhil, J. Hayakawa, X. Marti, J. Wunderlich, T. Jungwirth, and R. Bertacco, Appl. Phys. Lett. **102**, 192404 (2013).
[40] J. Nogués and I. K. Schuller, J. Magn. Magn. Mater. **192**, 203 (1999).
[41] A. E. Berkowitz and K. Takano, J. Magn. Magn. Mater. **200**, 552 (1999).
[42] A. Ghosh, S. Auffret, U. Ebels, and W. E. Bailey, Phys. Rev. Lett. **109**, 127202 (2012).
[43] Private communication. Data obtained by C. Cheng and W. E. Bailey of Columbia University, New York, for similar samples using a closed-cycle cryostat from 30 to 300 K, fitted with broadband FMR (2–18 GHz).
[44] R. Zhang and R. F. Willis, Phys. Rev. Lett. **86**, 2665 (2001).
[45] X. Y. Lang, W. T. Zheng, and Q. Jiang, Phys. Rev. B **73**, 224444 (2006).